Thermodynamic Investigation of Thin Films of Ethane Adsorbed on Magnesium Oxide

Thomas Arnold,† Richard E. Cook,‡ and J. Z. Larese*,†,‡

Oak Ridge National Laboratory, P.O. Box 2008, Oak Ridge, Tennessee 37831, and Department of Chemistry, University of Tennessee, Buehler Hall, Knoxville, Tennessee 37996

Received: August 31, 2004; In Final Form: January 10, 2005

The layering properties of ethane on MgO(100) were measured between 91 and 144 K using high-resolution adsorption isotherms. In contrast to previous studies, the results demonstrate that only three layers are formed. The thermodynamic functions derived from the data (isosteric heat, differential enthalpy, and entropy of adsorption) compare well with literature values and show a steady trend toward the bulk properties as the number of layers increased. Phase transitions for two of the layers were identified by monitoring the changes in the two-dimensional isothermal compressibility as a function of chemical potential. Both of these phase transitions occur at approximately 127 K and within 1 K of each other. Through the use of neutron diffraction, it is possible to identify at least one solid surface phase that melts at approximately 75 K. The transition at 127 K is therefore a transition between a liquidlike phase and a hyper-critical fluid. A comparison is made between the present data and our recent study of methane on MgO.

Introduction

Metal oxide (MO) and mixed metal oxide materials are some of the most important technological substances. MOs are used in commercial and medicinal applications that include sun blocks, pollution abatement, gastrointestinal antacids, sensors, optoelectronic devices, and catalysts/catalytic supports. Modifying and controlling the surface of MOs and understanding the interactions of adsorbed molecules at the gas−solid and liquid−solid interfaces are extremely important. The synthesis of thermally stable, well-defined and characterized nanometer-sized MO substrates is difficult; hence little is known about the structure and dynamics of thin hydrocarbon films adsorbed on their surfaces. We have recently developed methods to produce large quantities of high-quality, uniform MgO powders for use in molecular adsorption studies.[1] The adsorption properties of methane on MgO have been examined in great detail.[2−5] The purpose of this paper is to describe the absorption properties of ethane on the MgO(100) surface. It is the next step in our plan to systematically investigate the behavior of the short-chained alkanes and alkenes on MgO to develop a comprehensive theoretical description of how these molecules interact with the MgO(100) surface.

Previous studies[6] of the adsorption of ethane on both graphite and MgO have established some general features that are relevant to our measurements. The alkanes are strongly attracted to the graphite basal plane[7,8] and form monolayer solids that are predominately commensurate with it. The monolayer structure and subsequent layering behavior in these systems depends critically on the number of carbon atoms in the chain[9−15] and how densely packed the molecules are on the surface. This is a consequence of the competition between the molecule−substrate (M−S) and molecule−molecule (M−M) interactions. As the surface density is increased or as molecules begin to fill layers beyond the one closest to the substrate, the relative strength of the M−S compared to the M−M interactions dictates the details of the layering process.

While the complex phase behavior in the ethane-on-graphite system has been thoroughly examined by Taub[16−19] and others, information concerning the ethane on MgO system is more limited. Several years ago, Trabelsi and Coulomb (hereafter known as TC) published a thermodynamic study of ethane adsorbed on MgO that included a set of isotherm measurements and a comparison of thermodynamic quantities that they derived with ethane adsorption data on other surfaces (graphite and sodium chloride).[20] Suzanne et al. have performed an ultra high vacuum (UHV)-based structural study of monolayer, solid ethane films on MgO using low-energy electron diffraction (LEED).[21,22] In agreement with neutron diffraction data, they suggested that two, coverage-dependent solid phases, S1 and S2, form. The low-density phase (S1) is believed to adopt a structure with an oblique unit cell and a noticeable amount of positional and orientational disorder (presumably introduced by the square symmetry of the MgO). The higher-density phase (S2) adopts a $(2\sqrt{2} \times \sqrt{2})$ R45° herringbone structure. We note that a significant degree of uncertainty in these structural assignments exists. We aim to resolve these structural issues soon by performing a detailed diffraction and inelastic neutron scattering study. Here, we concentrate on describing our thermodynamic investigation.

Experimental Details

The MgO powders used in the studies described here were synthesized using a new process[1] that facilitates the production of large batches (∼20 g) of MgO powder that have a relatively narrow size distribution (250 ± 30 nm), large surface area (∼10 $m^2\ g^{-1}$), and almost exclusively (100) surface exposure.[1] These MgO powders meet all of the requirements needed to perform reliable surface adsorption studies. The details of the preparation method will be described in an upcoming paper. Throughout the production and sample preparation process, exposure of the MgO to air is minimal. The freshly produced material is heat-treated at 950 °C under high vacuum (10^{-7} Torr) before use. In

* Author to whom correspondence should be addressed. E-mail: jzl@utk.edu.
† Oak Ridge National Laboratory.
‡ University of Tennessee.

10.1021/jp046065w CCC: $30.25
Published on Web 04/19/2005

addition to the removal of any of the atmospheric molecules physisorbed on the surface during and shortly after the preparation, this heat treatment has previously been reported to homogenize the MgO(100) surface exposure.[23] The powder is handled and loaded into the sample cells under a dry argon atmosphere(~1 ppm of water vapor) and then sealed with indium wire. We have found that exposure to the atmosphere rapidly degrades the adsorption properties of the sample. The oxygen-free, high-conductivity (OFHC) sample cells used in these isotherm studies contain between 0.2 and 0.5 g of powder while the aluminum or vanadium cells used in complementary neutron investigations[24] contain around 7−15 g.

The high-resolution volumetric adsorption isotherms presented here were measured using an automated apparatus described previously,[25] generally following an experimental procedure that was used in our methane study.[5] For ethane, a data set consisting of more than 40 isotherms was measured with temperatures ranging between 91 K (the triple point) and 144 K. During the measurements, a Neocera LTC10 or LTC21 temperature controller combined with a silicon diode thermometer placed close to the sample position was used to keep the sample temperature constant within ±2 mK. Despite this extremely good temperature stability, there is a small difference between the actual sample temperature and the temperature controller setpoint. To determine the temperature offset, we filled the sample cell with the equivalent of ~40−50 layers of ethane at the conclusion of each isotherm. Once the gas equilibrated, we designated this pressure reading as the saturated vapor pressure (SVP) and then used the semiempirical Antoine eq 1 to set the sample temperature

$$\log_{10}(p) = B - \left(\frac{A}{T + C}\right) \tag{1}$$

The coefficients used in our calculations are $A = 791.3$, $B = 4.50706$, and $C = -6.422$[26,27] and give the vapor pressure (in bar) for ethane over the temperature range 91 K ≤ T ≤ 144 K. Finally, a dead space correction was applied to all of the vapor pressure isotherms to compensate for the ethane gas that occupies the sample volume but was not adsorbed on the MgO surface.

At the end of this paper, we also present preliminary neutron scattering data to illustrate our initial investigations of the structure and dynamics of the adsorbed ethane films. The data were obtained using the OSIRIS spectrometer at ISIS at the Rutherford Appleton Laboratory, U. K. The procedure for dosing the samples was very similar to the above, but we use a portable isotherm apparatus and the local cryogenic apparatus (liquid helium flow cryostats or closed-cycle refrigerators) together with a sample stick that allows reliable in situ gas dosing.[24]

Results and Discussion

Volumetric Adsorption Isotherm Results. To illustrate the data collected during our thermodynamic experiments, a representative volumetric isotherm recorded at 120.4 K is shown in Figure 1, in which it is easy to see two layering steps while a third is also distinguishable in the inset. The figure shows 20% of the measured (raw) data points together with an interpolated fit and its numerical derivative, determined using a commercial software package (Kaleidagraph). The interpolations have then been used to calculate the thermodynamic functions (two-dimensional isothermal compressibility and isosteric heat of adsorption) discussed below.

Using the same procedure as in our previous studies,[5,28] we used the numerical (first) derivative of an isotherm to precisely

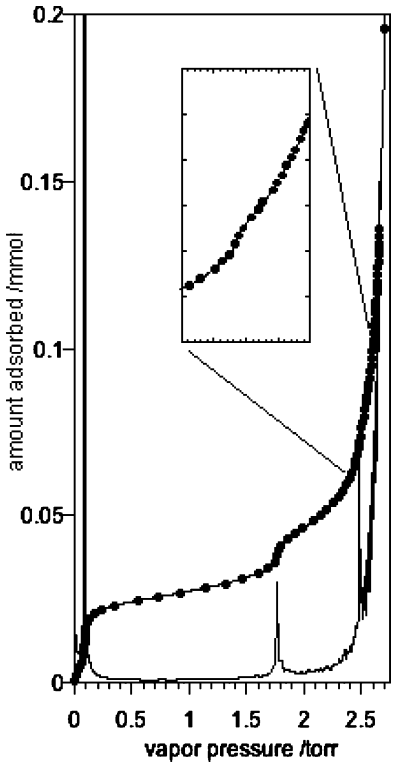

Figure 1. Volumetric isotherm of ethane on magnesium oxide at 120.4 K. Of the experimental data (●), 20% is plotted together with its interpolation and numerical derivative. The inset is a magnification of the third layering step.

determine the location of an adsorption step. For each layer, these positions are then plotted as a function of inverse temperature as follows

$$\ln(p(\text{Torr})) = B^{(n)} - \frac{A^{(n)}}{T} \tag{2}$$

where $A^{(n)}$ and $B^{(n)}$ are the coefficients determined from a linear fit for the nth layer adsorption step. Fits of the adsorption data to eq 2 for the nth layer are shown in Figure 2; the coefficients extracted from those fits are listed in Table 1. As the temperature is increased, identification of the third layer feature quickly becomes difficult, so only isotherms that showed clearly distinguishable third steps were used.

For a bulk liquid−vapor system, eq 2 is essentially the Clausius−Clapeyron relation. For an ideal (bulk) system, the coefficients can therefore be used to calculate the bulk enthalpy of vaporization. Although this relationship is widely used, its accuracy in describing experimental data for real systems over large temperature ranges has limitations. Consequently, there exists a number of variations of eq 2, including the Antoine equation.[29] With these limitations in mind, we will assume that the Clausius−Clapeyron relation is suitable as a first approximation to calculate some quantities that are relevant to our study of adsorbed layers.

The coefficients $A^{(n)}$ and $B^{(n)}$ derived for each layer can be used to calculate the differential enthalpy, $\Delta H^{(n)}$, and the differential entropy, $\Delta S^{(n)}$

$$\Delta H^{(n)} = -R(A^{(n)} - A^{(\infty)}) \tag{3a}$$

$$\Delta S^{(n)} = -R(B^{(n)} - B^{(\infty)}) \tag{3b}$$

Here, R is the gas constant (8.31 J mol^{-1} K^{-1}) and $A^{(\infty)}$ and

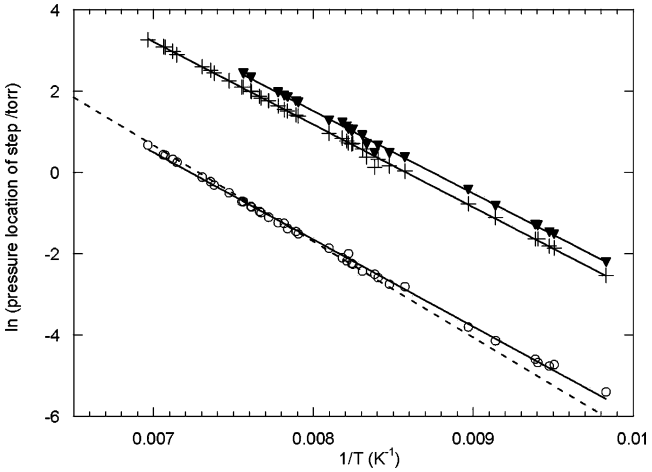

Figure 2. Clausius−Clapeyron plot of the positions of the adsorption steps for the three visible layers: (○) first layer, (+) second layer, and (▼) third layer. Linear fits are plotted through the data points, for which the fit parameters are listed in Table 1. Each of these fits has an *R*-value >0.99. The dotted line shows the corresponding fit derived from the coefficients given by TC.[20] The error in the measured pressure is negligible, although there is an uncertainty in determination of the SVP (and hence the temperature) of about 1% due to the asymptotic nature of the approach to SVP in an isotherm.

TABLE 1: Thermodynamic Properties Derived from the Clausius−Clapeyron Analysis as Described in the Text, the Parameters Derived from Our Methane Study,[5] and Those of TC[20] for Ethane on MgO

	$A^{(n)}$	$B^{(n)}$	Q_{ads}/kJ mol^{-1}	ΔH/kJ mol^{-1}	ΔS/J mol^{-1} K^{-1}
			Methane		
1	1385	15.307	11.511	−1.739	17.588
2	1212	16.880	10.069	−0.296	4.516
3	1176	17.040	9.773	0.000	3.190
4	1168	17.170	9.703	0.070	2.105
5	1165	17.220	9.685	0.088	1.688
∞	1176	17.423	9.773	N/A	N/A
			Ethane		
1	2142	15.482	17.800	−0.906	19.969
2	2035	17.454	16.911	−0.017	3.582
3	2029	17.740	16.861	0.033	1.205
∞	2034	17.9	16.894	N/A	N/A
			TC Ethane		
1	2363	17.2	19.659	−3.117	3.06
2	2085	17.9	17.330	−0.788	−2.68
3					
∞	1991	17.6	16.542	N/A	N/A

$B^{(\infty)}$ refer to the coefficients determined for the (SVP) bulk phase. These functions represent the difference between the "enthalpy (entropy) of vaporization" from the surface layer in question and that of the bulk. Hence, as the layers become more bulklike, $\Delta H^{(n)}$ and $\Delta S^{(n)}$ tend to zero. The values derived from our measurements are given in Table 1 and are compared with the values determined earlier by TC.

In our study, we find values of $A^{(2)}$, $A^{(3)}$, and $A^{(\infty)}$ are nearly constant, suggesting that there is little difference between the enthalpy of vaporization from the second and third layers and the bulk enthalpy of vaporization. We also note that the values of $\Delta S^{(n)}$ are all positive. Thus, the formation of the surface film is entropically favored relative to the formation of bulk crystallites (keeping in mind that both the entropies of adsorption and condensation are negative quantities). However, as the number of surface layers increases, the difference between the entropy of vaporization from the surface layers and the bulk system decreases in magnitude. Notably, $\Delta S^{(n)}$ approaches zero for the third layer.

The differential enthalpy and entropy obtained from the coefficients quoted by TC are noticeably different from our values, particularly in the first layer. Furthermore, TC's measured value of $\Delta S^{(1)}$ is significantly lower than the one reported here; in fact TC's $\Delta S^{(2)}$ is actually negative. Finally, TC's $\Delta H^{(n)}$ values are all more negative than the corresponding values reported here. In Figure 2, the dashed line that we have plotted corresponds to a Clausius−Clapeyron analysis *using the parameters derived in TC's study*. A comparison of the parameters from a Clausius−Clapeyron fit to our experimental data for the first layer with those derived from the TC study is found in Table 1. One sees that at high temperature there is reasonable agreement with our data, but at low temperature, where the measured pressure is very small (<0.5 Torr), we see a significant divergence. We will return to these discrepancies later in our discussion, but for now it is worth noting that unfortunately TC has not provided sufficient experimental details for us to determine the accuracy of their measurements. For our low-temperature measurements, we used a type 120AA Baratron high-accuracy absolute capacitance manometer from MKS calibrated between 0 and 100 Torr and with a minimum accuracy of 0.12% (the accuracy may be as good as 0.05%).[25,30] The error in our absolute temperature measurement is tied to the uncertainty in our measurement of the SVP and the accuracy of the Antoine equation fit, which we estimate to be no greater than 1%.

Enthalpy of Adsorption. The enthalpy of adsorption, ΔH_{ads} or Q_{ads}, can also be directly calculated from the Clausius−Clapeyron parameters and is given by

$$Q_{ads}^{(n)} = RA^{(n)} \tag{4}$$

The values that we obtained are shown in Table 1. In the high-coverage limit, this is equivalent to measuring the (temperature-dependent) bulk enthalpy of vaporization, ΔH_{vap}. We have determined that Q_{ads} for the second and third layers converge to a value of ∼16.9 kJ mol^{-1}, in good agreement with the bulk literature values (16.9 kJ mol^{-1} ≥ ΔH_{vap} ≥ 16.3 kJ mol^{-1} in the temperature range 120 K ≥ T ≥ 140 K[31]).

Another thermodynamic quantity of interest is the enthalpy of adsorption at constant surface coverage rather than simply at layer completion. Thus, the isosteric enthalpy of adsorption Q_{st} can be defined as

$$Q_{st} = RT^2 \left.\frac{\delta(\ln p)}{\delta T}\right|_{\theta} \approx RT^2 \frac{\Delta(\ln p)}{\Delta T} \tag{5}$$

Here, we use a numerical approximation of the partial derivative of ln p with respect to temperature at constant coverage, θ, by measuring the difference in ln p between two isotherms separated by a small temperature difference, ΔT, at exactly the same coverage. The accuracy of this approximation is dependent on the size of ΔT and the constancy of θ. It is experimentally impractical to perform isotherms where the data points are measured at exactly the same surface coverage at every temperature. Hence, it is necessary to use an interpolation of the data for these calculations.

Figure 3 shows the variation of Q_{st} as a function of surface coverage at 128.6 K. This trace is typical of the behavior of Q_{st} in the temperature interval 128 K < T < 142 K. We find that Q_{st} reaches its maximum of 24.5 ± 1.5 kJ mol^{-1} at a surface coverage (∼0.02 mmol) that corresponds to just below the completion of the first layer. There is also a clear indication in Figure 3 of a second peak near the completion of the second layer (∼18 ± 1.5 kJ mol^{-1}). However, as the film thickness

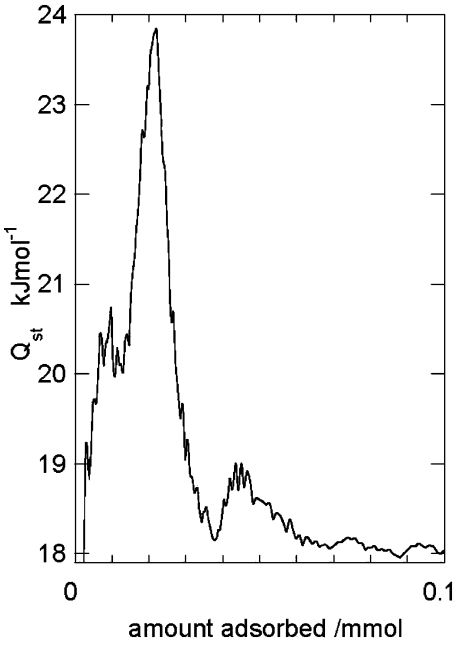

Figure 3. The isosteric heat of adsorption versus surface coverage for a typical isotherm at 128.6 K (solid line). The temperature interval, ΔT, used in calculating Q_{st} is ~1 K, and the temperature at which Q_{st} is quoted corresponds to the higher of the two values. Monolayer completion occurs at approximately 0.025 mmol. A large peak is visible at around 0.02 mmol with a smaller peak at approximately 0.045 mmol.

increases beyond two layers, the variation of Q_{st} with film thickness diminishes until it remains roughly constant above the third layer, converging on 17.5 ± 0.5 kJ mol^{-1}, in reasonable agreement with the bulk values quoted above.

We note that the peak value in Figure 3 is larger than the value obtained for the same layer using the Clausius−Clapeyron fit (17.8 kJ mol^{-1}), which reflects the temperature and coverage-dependent variation in the heat of adsorption. The value determined using the Clausius−Clapeyron method actually corresponds to an average value determined over the entire experimental temperature range and at approximately the coverage represented by the peaks in the numerical derivatives. Although it is considerably more difficult to get reliable data, the Q_{st} plot shown in Figure 3 is in our opinion the more definitive quantity to be reported.

A few comments about the variation of Q_{st} are appropriate. At low coverage, the ethane film forms a gaslike phase on the surface. As the density of this "lattice gas" increases, the likelihood of nearest-neighbor interactions increases, resulting in an increase in Q_{st}. There will be a coverage regime, where Q_{st} remains roughly constant, that corresponds to the formation of isolated patches of a condensed (solid or liquid) phase that gradually grows in size until the independent islands begin to interact. This interaction results in a slight film compression and a corresponding increase of Q_{st} up to a maximum value. Once the film reaches a maximum capacity in the layer (i.e., the layer nears completion), there will be a decrease in Q_{st}, corresponding to the increased difficulty of inserting molecules into the densely packed monolayer and the relative ease of promotion and condensation of molecules into a second layer. If the film continues to wet the surface, then presumably this process repeats itself.

Two-Dimensional Compressibility. The two-dimensional compressibility, K_{2D}, is a measure of the spreading pressure of individual layers and is a good indicator of phase changes within an adsorbed layer.[32] It is defined as

$$K_{2D} = \frac{(Ap)}{(N_A k_B T N^2)} \frac{dN}{dp} \tag{6}$$

where A is the total surface area of the substrate, p the pressure, N_A Avogadro's number, k_B Boltzmann's constant, and N is the number of adsorbed molecules. A plot of K_{2D} versus the reduced chemical potential for an isotherm measured at 120.4 K is shown in Figure 4. Three peaks arise from the three layering steps in the isotherm. The magnitude of the peaks is largest for the first layer and decreases in the second and third layers as a result of decreasing M−S interaction with increasing film thickness. This trend makes it difficult to observe peaks from the third layer. Both the intensity and the width of the K_{2D} peaks can be used as an indication of the phase of the adsorbed layer. For example, a solid layer would give an intense sharp peak while a liquid layer would give a relatively weak broad peak.[5,32]

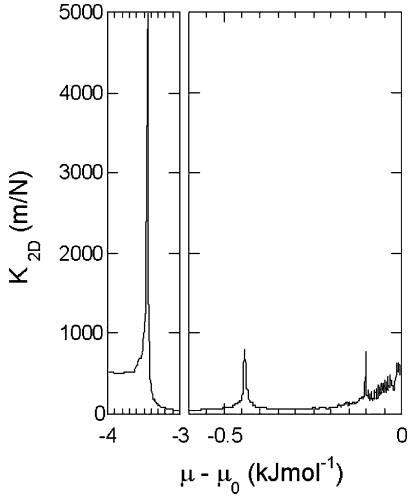

Figure 4. Two-dimensional compressibility versus reduced chemical potential $\mu - \mu_0$ for the isotherm shown in Figure 1. Three peaks are clearly visible, but there is no evidence of a fourth.

Within an individual layer, we can use K_{2D} to look for phase changes by monitoring the broadening of the compressibility peaks (Figure 5, parts a and b) as a function of temperature. Figure 5, parts c and d, show the full width at half-maximum (fwhm) of these features as a function of temperature for the first two layers (noise within our data does not allow for a dependable plot for the third layer).

At the lowest temperatures that we examined, the compressibility peaks are approximately constant in width and do not vary within the resolution of our measurement. At a certain temperature, the peaks begin to broaden at a rate approximately proportional to the increase in temperature. We find that the temperature at which the "broadening" occurs is independent of the specific sample used. A determination of the transition points for the monolayer and the bilayer film indicates that they both undergo a transition at roughly the same temperature. The first layer transition takes place at about 127 ± 1 K while the second is slightly higher at 127.5 ± 1 K. This temperature is 5−6 K lower than the 133 ± 1 K estimated by TC. These authors noted that their value is close to that of similar transitions of ethane on graphite (130 K)[10] and NaCl (132 K)[33] and suggested that it is independent of the substrate despite significant differences in terms of symmetry and crystal field. Our results suggest that there is a small substrate effect. The transition has previously been assigned as the two-dimensional (2D) layering critical temperature T_{2C} and can be thought of as

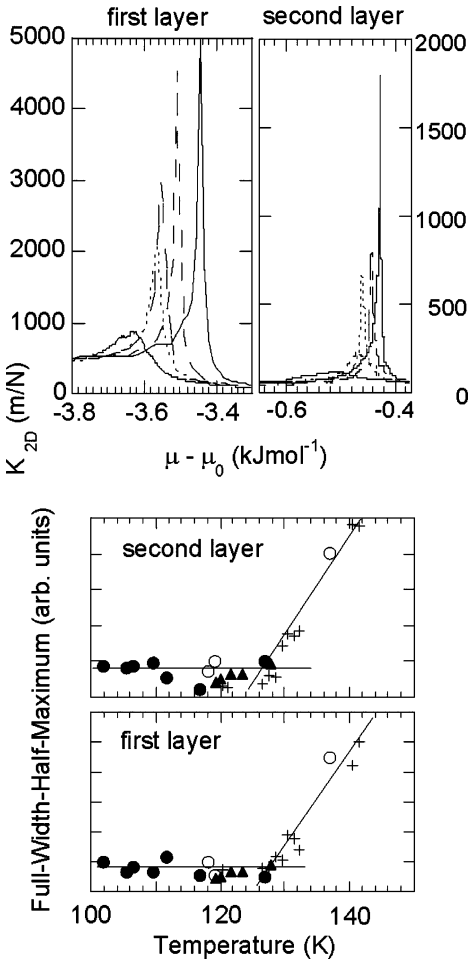

Figure 5. (Upper panel) Two-dimensional compressibility plots with varying temperature in the range 120 K $\leq T \leq$ 140 K, for (a) the first layer and (b) the second layer. (Lower panel) Plots of full width at half-maximum (fwhm) of the peaks in the two-dimensional compressibility, as a function of temperature: (c) first layer peaks and (d) second layer peaks. Each of the symbols (○, ●, +, and ▲) corresponds to a different sample, and the lines are drawn as guidelines. The 2D layering critical temperature T_{2C} for both the first and second layers occurs at approximately the same temperature 127 ± 1 K.

the transition from a 2D liquid to a 2D gas (specifically a 2D hypercritical fluid).

Neutron Diffraction Results. While the focus of the current work is thermodynamic, we have included a few relevant diffraction patterns of ethane on MgO from a preliminary structural study of the alkanes adsorbed on MgO. Diffraction patterns were collected over a range of temperatures for a surface coverage corresponding approximately to one complete layer. The patterns obtained at 90 and at 4.2 K are shown in Figure 6, respectively. The trace at 90 K shows a broad, weakly structured pattern, the peak of which lies in the region 1.4 Å$^{-1} \leq Q \leq$ 1.6 Å^{-1} (3.9 Å $\leq d \leq$ 4.5 Å), indicative of the presence of a largely disordered phase with a nearest-neighbor spacing of approximately 4.2 Å. Reduction of the temperature to 4.2 K results in the appearance of the highly structured pattern with numerous "sawtooth-shaped" diffraction peaks.[34−36] This is typical of a two-dimensional solid phase with long-range order. There are seven or eight discernible diffraction peaks (Table 2) that are not observable in Figure 6b, the most prominent of which are located at 1.48 ± 0.04 Å^{-1} and 1.67 ± 0.01 Å^{-1}. While some evidence of these two prominent features can be found in earlier data reported by Coulomb and Suzanne and their co-workers,[20−22] the statistical quality of this earlier data makes it difficult to

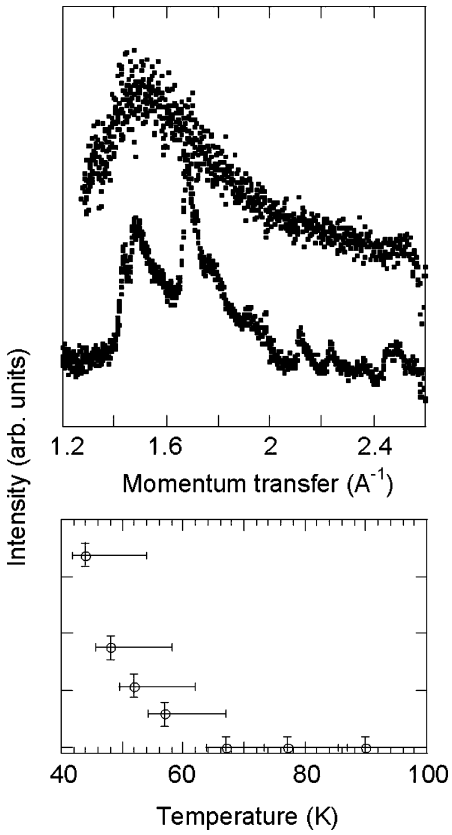

Figure 6. (Upper panel) Neutron diffraction patterns of ethane (θ = 1.2 layers) at 90 K (upper trace) and 4.2 K (lower trace). The patterns are shifted relative to each other for clarity, and the high temperature pattern was obtained over a shorter time (hence the greater noise). The visible peaks in the lower trace are listed in Table 2. There are some artifacts for the background subtraction in this figure, particularly at 2.6 Å^{-1}. (Lower panel) Plot of the peak intensity versus temperature for the diffraction peak at 1.67 Å^{-1}. We can approximately establish the monolayer melting point: 60 K $\leq T_m \leq$ 75 K. The errors in the temperature arose because there was no thermometer exactly at the sample position. The temperature was decreased at a steady rate with patterns taken over constant time intervals.

TABLE 2: Positions of the 2D Diffraction Peaks Observed in Our Recent Neutron Diffraction Study (OSIRIS), Compared with the Peaks Previously Reported and Their Assignments[a]

currently observed momentum transfer/Å^{-1}	previously observed[20−22] momentum transfer/Å^{-1}	index according to the S2 unit cell (a = 8.43, b = 4.21) ◆◇
out of measured range	0.745 ◇	(1,0)
1.44		
1.48 ± 0.04	1.497 ◆◇	(2,0) or (0,1)
1.67 ± 0.01	1.671 ◆◇	(1,1)
1.71		
1.78		
1.91 ± 0.01		
2.11 ± 0.01	2.1 ◇	(2,1)
2.23 ± 0.01	2.25 ◇	(3,0)
2.36		
2.45		
2.48 ± 0.04		

[a] We observe several more peaks than previously seen. The peaks without the indication of an error are more ambiguous: ◆ = neutron diffraction;[20] ◇ = LEED.[21,22]

identify any other features with certainty. The lower intensity peaks observed in the current study were not resolvable previously. Coulomb, Suzanne, and co-workers associated these prominent peaks with the S2 phase described in the Introduction

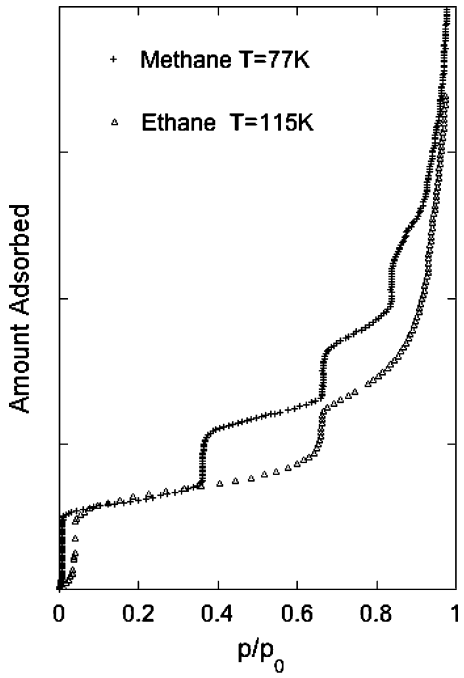

Figure 7. Volumetric isotherms of methane (+, 77 K) and ethane (△, 120.4 K) measured on the same sample of magnesium oxide. For clarity, only 20% of the data points are shown. P_0 is the saturation vapor pressure for each sample gas at the temperature of the isotherm. Note that the ethane isotherm is scaled by a factor of 1.264 to match the monolayer height of the methane isotherm.

(C−C molecular axis parallel to the MgO surface). The marked statistical improvement in the present diffraction data is most likely due to the chemical purity, size uniformity, and mean size of the MgO particles as was noted in our earlier findings[3,28] as well as the high flux and appropriately matched resolution of the instrument used here (OSIRIS). As we noted above, our complete structural analysis of the ethane on MgO(100) system will appear in a later publication coupled with inelastic neutron scattering data to further clarify the solid structure.

We monitored the intensities of these more intense diffraction peaks while slowly cooling the sample (∼ 0.2 K/min); this is shown in Figure 6. We note that over the range 60 K ≤ T ≤ 75 K a marked increase in the scattered intensity takes place in the appropriate Q ranges, establishing an approximate freezing (melting) point of the S2 phase. Detailed heat capacity measurements are planned to accurately determine the ethane on MgO phase diagram (including the S1 to S2 transition).

For reference, the bulk (three-dimensional) melting point of ethane is 90 K while its boiling point is 184.5 K. Studies of monolayer melting on graphite indicate that as a rule of thumb 2D crystals melt at a temperature approximately equal to 70% of the bulk melting point. The results presented here appear to follow this trend. We also note that the 2D liquid to 2D gas transition (at ∼127 K) discussed above occurs at approximately 70% of the bulk boiling point.

Comparison with Methane Adsorbed on Magnesium Oxide. One of our objectives is to understand the interaction of the normal alkanes with MgO. We therefore compare our results for ethane and methane. Figure 7 shows typical methane and ethane isotherms measured on the same sample with exactly the same isotherm apparatus. Two features immediately stand out. First, ethane has only three discernible isotherm steps; methane has up to seven.[5] We have been unable to confirm the observation of five layers in ethane made by TC. We note that although there is appreciable noise visible in the plot of K_{2D} for the third layer of ethane on MgO, as a result of ∼2 mK temperature fluctuations during an isotherm measurement, we have the same experimental temperature stability as in the methane experiments. In the course of our research, we have established that methane isotherms can be used as a test for the MgO quality. Preliminary methane isotherms performed on each of the samples used here clearly showed (at least) five steps, giving us confidence that the samples were of a high standard. Meanwhile, methane isotherms performed by Gay, Suzanne, and Coulomb[37] using their MgO samples only visibly show four steps. On this basis, we would expect that steps as well-defined as those suggested by TC would be clearly visible in our isotherms.

The second distinctive feature is the relative "heights" of the monolayer steps. Not surprisingly, the number of molecules needed to complete the first layer of ethane is lower than for methane. This is understandable from molecular area considerations if ethane adsorbs with its C−C bond parallel to the surface. Through the use of the extensive data that exists for the methane/MgO system, including neutron diffraction and rotational tunneling spectroscopy,[2−4] we can confidently establish that the area per molecule (APM) for a monolayer of solid methane on MgO at 77 K is 17.72 Å^2. Through the use of this information and the ethane isotherm performed on the same MgO sample (i.e., one with a known surface area), we can readily calculate the APM of ethane on MgO at 120.4 K to be 22.40 Å^2.

At 77 K, the methane layer is a solid phase, while we have already established that at 120 K the ethane film is in a disordered state. We can use the momentum transfer location of the broad feature in the diffraction pattern at 90 K (Figure 6) to estimate an APM of approximately 20 Å^2 (based on the intermolecular spacing of 4.5 Å). Allowing for the thermal expansion of the 2D liquid over the 90−120 K temperature range, we believe that our estimate of an APM of 22.4 Å is reasonable. The area calculated for the $(2\sqrt{2} \times \sqrt{2})$ R45° herringbone structure proposed by Suzanne et al.[21,22] is the same as that for methane, 17.72 Å^2. Unfortunately, due to the low vapor pressures that exist in the 2D solid regime, we cannot use our isotherm apparatus to independently confirm this value.

Finally, we can compare the thermodynamic quantities determined here with the equivalent values calculated from our methane data (both shown in Table 1). We note that Q_{ads}(ethane) > Q_{ads}(methane) in line with the bulk heats of vaporization. We also see that the trend in the values of $\Delta H^{(n)}$ and $\Delta S^{(n)}$ is the same for both methane and ethane, the difference being that the layering extends over five layers in methane instead of three. In ethane, $\Delta H^{(2)}$ was effectively the same as the enthalpy of vaporization of bulk ethane. This does not occur for methane until the third layer. Meanwhile, the entropic influence in methane extends to the higher layers and only approaches zero for the fifth (or perhaps sixth) layer.

There are two important points to keep in mind when considering why the differences arise in the layering properties of methane versus ethane on MgO. First, complete layering or wetting requires that a film grow to macroscopic dimensions. This usually means that the surface needs to act as a near perfect template for the growing film. Next, a strong substrate interaction has a greater impact on a nonspherical molecule through the imposition of a molecular orientation close to the interface that is incompatible with any of the bulk crystal planes. It is known that the structure of (100) bulk methane solid is almost a perfect match with the MgO(100) surface. Hence, the layer-by-layer growth observed for methane on MgO is not surprising

since there is essentially no mismatch (and hence no strain energy) between the surface phase and the bulk. It has been shown that the tetrahedral symmetry of the methane molecule and the 4-fold symmetry of the MgO(100) surface are structurally compatible at low temperature since the molecule sits with the C_{2v} axis perpendicular to the (100) surface plane. It has also been found that the molecule is rotationally disordered at temperatures above 20 K and undergoes unhindered, nearly spherical reorientations.[3,38,39] These are conditions that minimize any substrate-imposed orientational order (strain) on the molecular solid film growth.

The situation is not the same for ethane. The structure of bulk solid ethane is still poorly defined.[40] X-ray crystallographic studies find that at least two different solid phases (with considerable molecular disorder) exist above and below 90 K. Both of these solid crystal phases have structures that are poorly matched to the MgO(100) surface structure (even in the quasi-cubic form), and this makes it additionally difficult for a uniform solid film to form beyond those closest to the MgO surface. From our study of the heats of adsorption and from the diffraction data, it appears to be energetically favorable to form a monolayer solid and several layers of liquid. This benefit no longer appears to exist in the formation of multilayer solid ethane films. This is illustrated in our adsorption studies directly. Table 1 illustrates that the thermodynamic differences between the adsorbed phase and the bulk phase decreases as the layer thickness increases. This is a direct indication that the molecular interactions experienced by a molecule in the *n*th layer ($n > 1$) become more like those experienced by a molecule within the bulk phase.

Conclusions

We have performed a thermodynamic investigation of the layering properties of ethane on MgO(100) surfaces between 91 and 144 K on high-quality MgO(100) surfaces. Within this temperature range, we observe three distinct layering transitions. Using the temperature dependence of the location and width of these transitions, we have identified that for layers one and two a phase transition takes place in the neighborhood of 127 K.

Using neutron diffraction, we have identified the formation of at least one solid phase at temperatures below 75 K. By following the temperature dependence of the diffracted intensity, we are able to establish that the thermodynamic transition that we observe at 127 K is one proceeding from a phase with short-range spatial order (liquid). We have not yet characterized the nature of the dynamics associated with this phase but expect to perform quasi-elastic neutron scattering investigations to identify the microscopic nature of the translational diffusion in this regime. At higher coverage, we note that the isosteric heat in this temperature regime converges to a value that is close to the bulk ethane heat of vaporization.

Acknowledgment. The authors would like to thank L. L. Daeman, R. J. Hinde, and J. M. Hastings for useful discussions and S. M. Clarke for his contributions to the neutron diffraction component of this work. In addition, we would like to thank Tim Free for his machinist skills and John Dreyer, Richard Down, Andrew Church, Jon Bones, and other members of the ISIS user support group for their contributions to this work performed at ISIS. This work was performed with the support of the University of Tennessee, Knoxville, and the Division of Materials Sciences, Office of Basic Energy Sciences, U. S. Department of Energy, under Contract No. DE-AC05-00OR22725 with Oak Ridge National Laboratory, managed and operated by UT−Battelle, LLC.

References and Notes

(1) Kunnmann, W.; Larese, J. Z. U.S. Patent 6,179,897, 2001.
(2) Larese, J. Z.; Hastings, J. M.; Passell, L.; Smith, D.; Richter, D. *J. Chem. Phys.* **1991**, *95*, 6997.
(3) Larese, J. Z. *Physica B* **1998**, *248*, 297.
(4) Larese, J. Z.; Marero, D. M. Y.; Sivia, D. S.; Carlile, C. J. *Phys. Rev. Lett.* **2001**, *87*, 206102.
(5) Freitag, A.; Larese, J. Z. *Phys. Rev. B* **2000**, *62*, 8360.
(6) Bruch, L. W.; Zaremba, E.; Cole, M. W. *Physical Adsorption: Forces and Phenomena*; Oxford University Press: New York, 1997.
(7) Clarke, S. M. *Curr. Opin. Colloid Interface Sci.* **2001**, *6*, 118.
(8) Groszek, A. J. *Proc. R. Soc. London, Ser. A* **1969**, *314*, 473.
(9) Hamilton, J. J.; Goodstein, D. L. *Phys. Rev. B.* **1983**, *28*, 3838.
(10) Regnier, J.; Menaucourt, J.; Thomy, A.; Duval, X. *J. Chim. Phys.* **1981**, *78*, 629.
(11) Zhao, X.; Kwon, S.; Vidic, R. D.; Borguet, E.; Johnson, J. K. *J. Chem. Phys.* **2002**, *117*, 7719.
(12) Herwig, K. W.; Newton, J. C.; Taub, H. *Phys. Rev. B* **1994**, *50*, 15287.
(13) Alkhafaji, M. T.; Migone, A. D. *Phys. Rev. B* **1996**, *53*, 11152.
(14) Arnold, T.; Dong, C. C.; Thomas, R. K.; Castro, M. A.; Perdigon, A.; Clarke, S. M.; Inaba, A. *Phys. Chem. Chem. Phys.* **2002**, *4*, 3430.
(15) Arnold, T.; Thomas, R. K.; Castro, M. A.; Clarke, S. M.; Messe, L.; Inaba, A. *Phys. Chem. Chem. Phys.* **2002**, *4*, 345.
(16) Newton, J. C.; Taub, H. *Surf. Sci.* **1996**, *364*, 273.
(17) Suzanne, J.; Seguin, J. L.; Taub, H.; Biberian, J. P. *Surf. Sci.* **1983**, *125*, 153.
(18) Zhang, S.; Migone, A. D. *Phys. Rev. B.* **1990**, *42*, 8674.
(19) Zhang, S.; Migone, A. D. *Surf. Sci.* **1989**, *222*, 31.
(20) Trabelsi, M.; Coulomb, J. P. *Surf. Sci.* **1992**, *272*, 352.
(21) Sidoumou, M.; Angot, T.; Suzanne, J. *Surf. Sci.* **1992**, *272*, 347.
(22) Hoang, P. N. M.; Girardet, C.; Sidoumou, M.; Suzanne, J. *Phys. Rev. B* **1993**, *48*, 12183.
(23) Cox, P. A.; Hendrich, V. E. *The Surface Science of Metal Oxides*; Cambridge University Press: New York, 1994.
(24) Koehler, C. F.; Larese, J. Z.; Rodriguez, J. A.; Jirsak, T.; Freitag, A.; Hanson, J. C.; Chaturvedi, S. *Rev. Sci. Instrum.* **1999**, *62*, 113.
(25) Mursic, Z.; Lee, M. Y. M.; Johnson, D. E.; Larese, J. Z. *Rev. Sci. Instrum.* **1996**, *67*, 1886.
(26) *NIST Chemistry WebBook*; Linstrom, P. J., Mallard, W. G., Eds.; NIST Standard Reference Database 69; National Institute of Standards and Technology: Gaithersburg, MD, 2003 (http://webbook.nist.gov).
(27) Carruth, G. F.; Kobayashi, R. *J. Chem. Eng. Data* **1973**, *18*, 115.
(28) Sprung, M.; Larese, J. Z. *Phys. Rev. B* **2000**, *61*, 13155.
(29) Rowlinson, J. S.; Swinton, F. L. *Liquids and Liquid Mixtures*, 3rd ed.; Butterworths: Boston, 1982.
(30) Baratron capacitive nanometers. MKS Instruments Inc.: Andover, MA.
(31) Younglove, B. A.; Ely, J. F. *J. Phys. Chem. Ref. Data* **1987**, *16*, 577.
(32) Larher, Y.; Angerand, F. *Europhys. Lett.* **1988**, *7*, 447.
(33) Ross, S.; Clark, H. *J. Am. Chem. Soc.* **1954**, *76*, 4291.
(34) Warren, B. E. *Phys. Rev.* **1941**, *59*, 693.
(35) Warren, B. E.; Bodenstein, P. *Acta Crystallogr.* **1966**, *20*, 602.
(36) Wilson, A. J. C. *Acta Crystallogr.* **1949**, *2*, 245.
(37) Gay, J. M.; Suzanne, J.; Coulomb, J. P. *Phys. Rev. B* **1990**, *41*, 11346.
(38) Larese, J. Z. Unpublished work.
(39) Gay, J. M.; Stocker, P.; Degenhardt, D.; Lauter, H. J. *Phys. Rev. B.* **1992**, *46*, 1195.
(40) van Nes, G. J. H.; Vos, A. *Acta Crystallogr., Sect. B* **1978**, *34*, 1947.